nature materials

LETTERS

https://doi.org/10.1038/s41563-019-0356-x

In situ probing electrified interfacial water structures at atomically flat surfaces

Chao-Yu Li[1,3], Jia-Bo Le[1,3], Yao-Hui Wang[1], Shu Chen[2], Zhi-Lin Yang[2], Jian-Feng Li[1,2*], Jun Cheng[1*] and Zhong-Qun Tian[1]

Solid/liquid interfaces are ubiquitous in nature and knowledge of their atomic-level structure is essential in elucidating many phenomena in chemistry, physics, materials science and Earth science[1]. In electrochemistry, in particular, the detailed structure of interfacial water, such as the orientation and hydrogen-bonding network in electric double layers under bias potentials, has a significant impact on the electrochemical performances of electrode materials[2–4]. To elucidate the structures of electric double layers at electrochemical interfaces, we combine in situ Raman spectroscopy and ab initio molecular dynamics and distinguish two structural transitions of interfacial water at electrified Au single-crystal electrode surfaces. Towards negative potentials, the interfacial water molecules evolve from structurally 'parallel' to 'one-H-down' and then to 'two-H-down'. Concurrently, the number of hydrogen bonds in the interfacial water also undergoes two transitions. Our findings shed light on the fundamental understanding of electric double layers and electrochemical processes at the interfaces.

Electrochemical interfaces—buried between electrodes and electrolytes—are notoriously difficult to probe, and enormous efforts, both experimentally and computationally, have been devoted to this endeavour[5–9]. Although some progress has been made, the microscopic structures of electrochemical interfaces remain elusive and a great challenge in physical sciences. For example, radiation source-based X-ray techniques have been used to investigate the interfacial water structure in the first approximately two to three molecular layers close to electrode surfaces[5,8]. By employing an X-ray scattering technique[5], the water density distribution profile in the first water layer on a Ag electrode surface has been revealed, and the corresponding averaged water density is dependent on the bias potential. Others have characterized the hydrogen-bonding structures of liquid water with X-ray absorption spectroscopy[10,11] and have studied the water interface[8] and found that dangling O–H bonds exist in the interfacial water on both negatively and positively charged Au surfaces.

Vibrational spectroscopies, such as infrared, sum-frequency generation (SFG) and Raman spectroscopy, are used in investigating the nature of O–H bonds and the chemical environment of interfacial water[12–15], and have been widely used in electrochemistry. Plasmon-enhanced Raman spectroscopies, in particular, have unique advantages in extracting the fingerprint vibrational signatures of adsorbed species, even at very negative potentials accompanied by extensive solvent reactions[15]. Several structural models of interfacial water have been proposed based on vibrational spectroscopic measurements, partly because of the ambiguity in interpreting the spectra[12,16,17]. So far, tetrahedrally coordinated water[18,19], trihedrally coordinated water[18,19], surface specifically adsorbed water[14], hydrophobic water[17] and so on have been reported at metal/water interfaces using various vibrational spectroscopy techniques. However, a clear picture of how these types of interfacial water change in response to the applied potential is still missing[14,17,20].

Here, aiming to unravel the structures of interfacial water in electric double layers (EDLs), we combine in situ Raman spectroscopy and ab initio molecular dynamics (AIMD) to study interfacial water at Au single-crystal electrodes under bias potentials. Both experiment and theory have indicated two transitions in the O–H stretching vibrational modes of interfacial water when sweeping to negative potentials, which can be attributed to transitions in water configurations in EDLs.

The in situ electrochemical shell-isolated nanoparticle-enhanced Raman spectroscopic (SHINERS) technique was carried out to investigate interfacial water at atomically flat electrode surfaces (Fig. 1a). As calculated by the three-dimensional finite-difference time-domain (3D-FDTD) method (Fig. 1b), Raman signal enhancement (G) in the 'hot spot' between the Au SHIN and a single-crystal surface is more than six orders of magnitude, greatly magnifying the signals from interfacial water at Au electrode surfaces (see Supplementary Fig. 1 for electron microscope characterization of SHINs). Furthermore, to obtain the atomic structure of interfacial water we used AIMD to simulate an EDL at the Au/water interface. As an important complementary tool, AIMD has recently been used to investigate water structures[8] and electronic energy levels[21] at electrochemical interfaces. The recently developed computational standard hydrogen electrode method[21,22] in particular enables us to determine the electrode potentials of simulated interface models, making it possible to link the AIMD structures to realistic electrochemical conditions. Figure 1c presents a schematic representation of an EDL at a Au(111)/aqueous solution interface according to the Stern model (the Gouy–Chapman layer can be omitted under high ionic strength conditions); an electric field, screened by the interfacial water, is generated by the charged metal surface and outer Helmholtz layer (OHP).

Figure 2a,b shows the Raman spectra of the O–H stretching mode ($\nu_{O\text{-}H}$) and H–O–H bending mode ($\delta_{H\text{-}O\text{-}H}$) of interfacial water at the Au(111) surface, measured by in situ electrochemical Raman spectroscopy (the libration modes are shown in Supplementary Fig. 2), in which the corresponding electrode potential is referred to

[1]State Key Laboratory of Physical Chemistry of Solid Surfaces, Collaborative Innovation Center of Chemistry for Energy Materials (iChEM), MOE Key Laboratory of Spectrochemical Analysis and Instrumentation, College of Chemistry and Chemical Engineering, Xiamen University, Xiamen, China. [2]Department of Physics, Xiamen University, Xiamen, China. [3]These authors contributed equally: Chao-Yu Li, Jia-Bo Le *e-mail: li@xmu.edu.cn; chengjun@xmu.edu.cn

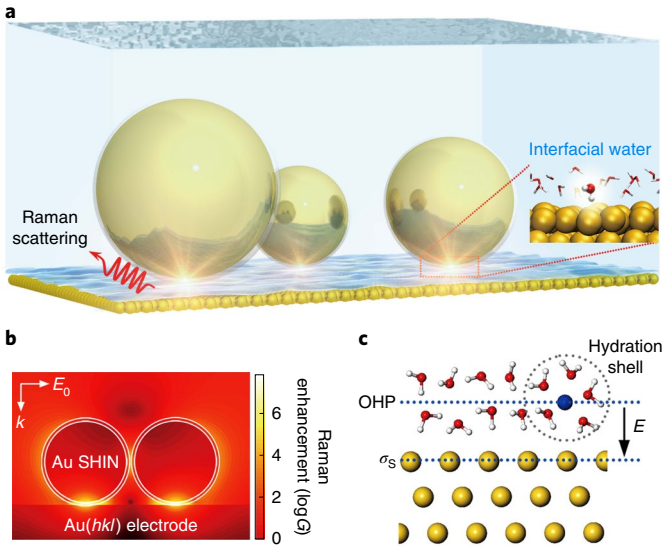

Fig. 1 | Probing interfacial water on Au single-crystal electrode surfaces. **a**, Schematic illustration of the Au shell-isolated nanoparticles (SHINs)–single-crystal surface coupling mode, in which 'hot spots' of the electric field largely enhance the Raman signals of water at the interface. **b**, 3D-FDTD calculation of the Raman enhancement distribution of the coupling configuration between the Au surface and a 2×2 array of Au SHINs, where k and E_0 denote the wavevector and electric field of incident light, respectively. **c**, Schematic representation of an EDL model, where Au, O, H and Na atoms are yellow, red, white and blue. σ_s, OHP and E represent surface charge density, outer Helmholtz plane and electric field.

the potential of zero charge (PZC) of Au(111) (that is, 0.29 V versus Ag/AgCl; ref. [23]). We are able to separate each spectrum into three Gaussian peaks with good fitting coefficients (the three peaks are plotted separately in Supplementary Fig. 3), indicating that three different kinds of water are present at the interfaces; similar assignments have also been suggested in the literature[8,14,17–19]. As shown in Supplementary Fig. 4, the same decomposition can also be applied to the spectra measured at the Au(100) surface. In Fig. 2a,c we notice that both the frequencies and intensities of the three peaks show a strong dependence on the electrode potential, suggesting that the obtained Raman signals mainly come from the first few water layers close to the metal surface[14]. We assign the peak at a higher wavenumber (~3,600 cm^{-1}) to the dangling O–H bonds of the interfacial water, consistent with the assignment recently reported by X-ray absorption spectroscopy (XAS)[8] and SFG[17] measurements on the Au electrode. The peaks at ~3,450 and ~3,300 cm^{-1} were attributed to trihedrally and tetrahedrally coordinated water at the interface based on previous SFG results from quartz/water[18] and metal/water[14,19,24] systems. We further analysed the intensity change of these three peaks along with the potential shift, as illustrated in Fig. 2c. We first notice that the intensity of the trihedrally coordinated water dominates over the whole potential range, suggesting that the interfacial water mainly consists of trihedrally coordinated water on Au(111)[19,24]. Furthermore, the intensities of trihedrally and tetrahedrally coordinated water show a similar trend; both show a dramatic increase when the potential sweeps from −0.29 to −1.29 V and are reduced to ~70% of the maximum value and almost zero, respectively, when the potential drops below −1.29 V. Also, we find that the intensity of the dangling O–H bonds shows a steep increase at potentials below −1.68 V.

It is even more interesting to note the potential dependence of the Raman frequency of the interfacial water at the Au(111) surface, as shown in Fig. 2e. A general decrease is seen towards the negative potential as well as two distinct transitions at −1.29 V and −1.85 V. A similar transition in the Stark tuning rate of $\nu_{O\text{-}H}$ was previously observed at the Ag electrode[20]. We attribute the negative shift of the Raman frequency to the Stark effect[25], while the observed transitions are not well recognized before. It is dependent on the surface, as these transitions cannot be found at the Au(100) or nanoparticles surface[20]. Also, the libration mode reveals an increasing intensity during the transitions (Supplementary Fig. 2b), which indicates an ordered structure of interfacial water on electrified electrode surfaces[16]. To elucidate these two transitions, AIMD simulations were used to model the Helmholtz double layers at the Au(111)/water interface at potentials negative to the PZC. In the AIMD models (Fig. 1c and Supplementary Fig. 5), Na^+ ions serve as counterions, compensating the negative charges at the electrode surface. The Au(111) surfaces are H-free in all the models, as indicated by the Raman experiments, in which no Au–H stretching mode is observed. As illustrated in Supplementary Fig. 6, the EDL capacitance obtained from the calculated charging curve is in good agreement with the experimental value[23], which supports that our EDL models are reasonable representations of the electrochemical conditions. Figure 2d shows the calculated velocity density of states (VDOS) of interfacial water corresponding to $\nu_{O\text{-}H}$ at different potentials, and the frequencies of the peak area as a function of potential are plotted in Fig. 2e for comparison with the Raman experiments. Although constraints on the set-up of EDL models and the computing costs limit the number of data points (grey triangles in Fig. 2e) obtained from AIMD simulations, the trend generally fits the Raman data, in which two turning points at potentials around −1.3 V and −1.9 V can be roughly identified. These two turning points separate the potential range down to ~−2.13 V into three regions (Fig. 2e); the Stark tuning rate in region II (−1.3 V to ~−1.9 V) is significantly larger than those in regions I (above −1.3 V) and III (below −1.9 V).

The good agreement achieved between the experimental and simulated spectra is encouraging, and we further investigated how the water structures in the EDLs change at different potentials. The distribution profiles of oxygen density (ρ_O), hydrogen density (ρ_H) and dipole orientation ($\rho_O \cos\varphi$, where φ is the angle between the surface normal and the bisector of the water molecule) along the direction normal to the surface are shown in Fig. 3a. To further elucidate the water orientation in the EDLs we also analysed the probability distributions of φ and the angle between the surface normal and O–H bond direction (denoted by θ), as plotted in Fig. 3b. We first note that at PZC the interfacial water bears little net orientation dipole (Fig. 3a); moreover, most of the water has both distributions of θ and φ centred around 90° (Fig. 3b), indicating that these water molecules adopt a geometry with molecular planes nearly parallel to the surface (denoted as 'parallel' water). At a potential of −1.34 V, a sharp peak at ~140° in the φ distribution is observed around the transition between regions I and II, and two sharp peaks with similar abundance are found at ~90° and ~160° in the θ distribution, corresponding to a water structure with one O–H bond nearly parallel to the surface and the other H atom pointing almost straight down to the surface (denoted as 'one-H-down' water). The observation of the 'one-H-down' water is consistent with a previous study on gold electrodes using XAS[8].

We further studied how the hydrogen bonding of interfacial water at the Au(111) surface changes with the applied potential. As shown in Fig. 4, when the potential shifts from PZC to −1.34 V in region I, we find that the number of hydrogen-bond donors (N_{donor}) of the interfacial water decreases from ~1.5 to ~1, indicating that the interfacial water is gradually turning from the 'parallel' to the 'one-H-down' configuration. The existence of one remaining hydrogen-bond donor suggests that the interfacial water forms hydrogen-bond networks with neighbouring water via the parallel O–H bond at −1.34 V, as shown in the inset of Fig. 4. Due to the presence of

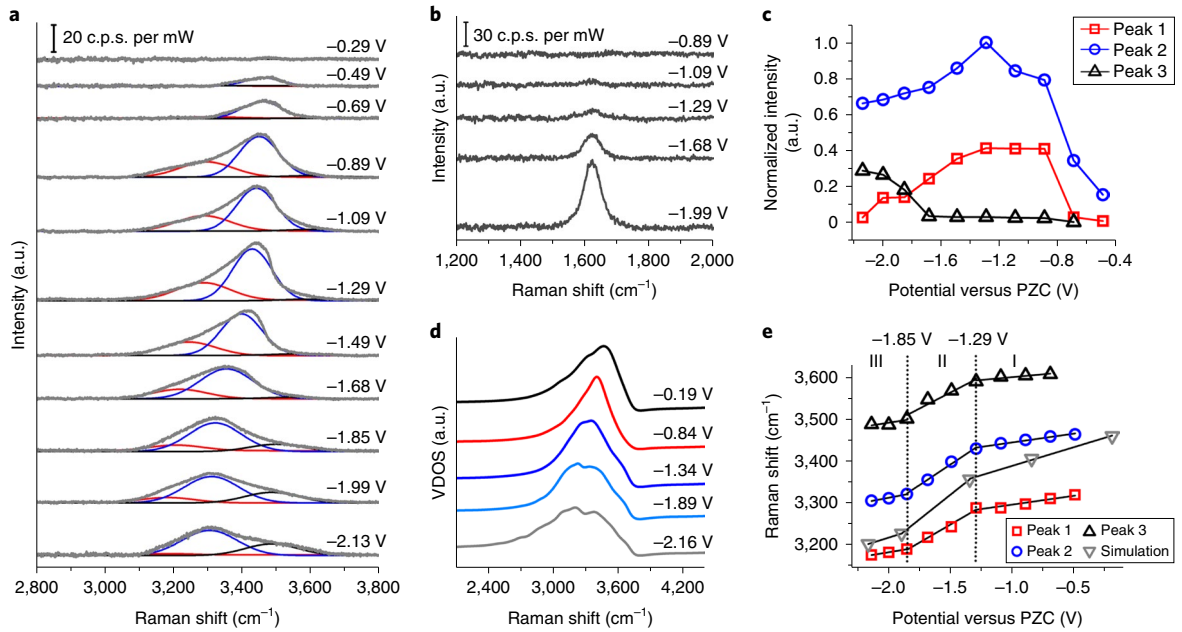

Fig. 2 | Vibrational spectra of interfacial water at Au single-crystal electrode surfaces. a, In situ electrochemical Raman spectra (grey curves) of the O–H stretching mode at the Au(111) surface measured in 0.1 M Na_2SO_4 solution. These are fitted with three gaussians (red, blue and black, respectively). **b**, Raman spectra of the H–O–H bending mode of interfacial water at the Au(111) surface. **c**, Intensities of the three peaks of interfacial water at the Au(111) electrode surface. Peaks 1, 2 and 3 correspond to the fitted Raman peaks with the small, medium and large wavenumbers shown in **a**, respectively. The intensities of the three peaks are normalized with respect to the maximum value of peak 2. **d**, VDOS corresponding to the O–H stretching mode of interfacial water at the Au(111) surface. **e**, Comparison of experimental and calculated frequencies of the O–H stretching mode of interfacial water as a function of the applied potential at the Au(111) surface. The data points in regions I, II and III are linearly fitted.

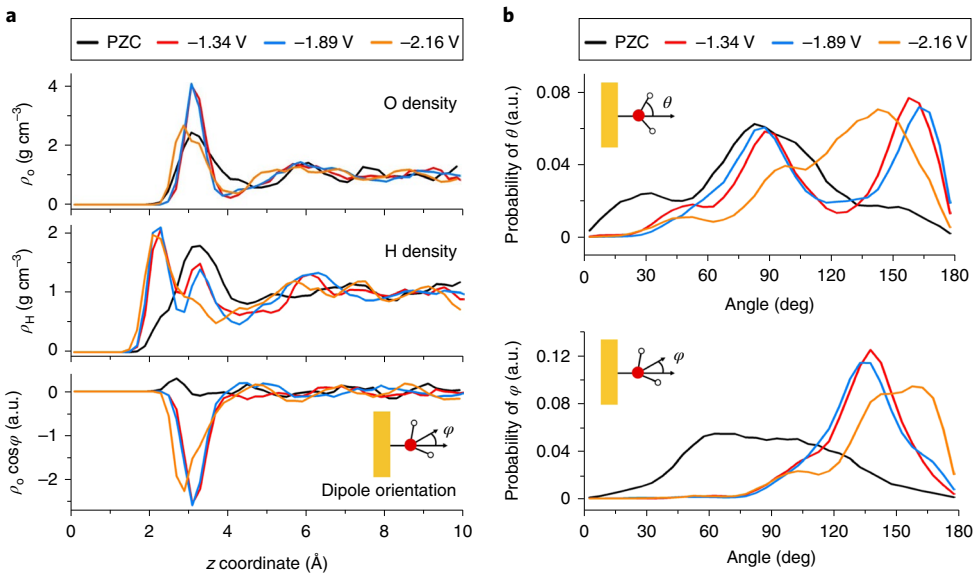

Fig. 3 | Potential dependence of the interfacial water structure at the electrified Au(111) surface from AIMD simulations. a, Profiles of oxygen density (upper), hydrogen density (middle) and dipole orientation of H_2O (lower) along the surface normal direction z, where the zero corresponds to the location of the metal surface. The potentials are referenced to the PZC of the Au(111) surface. The curves represent the averages of two symmetric interfaces in the EDL models shown in Supplementary Fig. 5. **b**, Calculated probability distributions of angle θ between the O–H bond of water and the surface normal (upper) and angle φ between the water bisector and the surface normal (lower) of the interfacial water. Both angles are shown in the insets, and the interfacial water is defined as being within 4 Å of the metal surface, as suggested in the density profiles in **a**. The results at other potentials are provided in Supplementary Figs. 7 and 8.

the Au(111) surface, the water in the first layer is mostly trihedrally coordinated, in line with the observed high Raman intensity of this water (peak 2 in Fig. 2c). Based on the selection rule and electromagnetic enhancement mechanism[12,26], the Raman intensity of the 'one-H-down' water should be stronger than the 'parallel' water. Shifting to more negative potentials will reorient 'parallel'

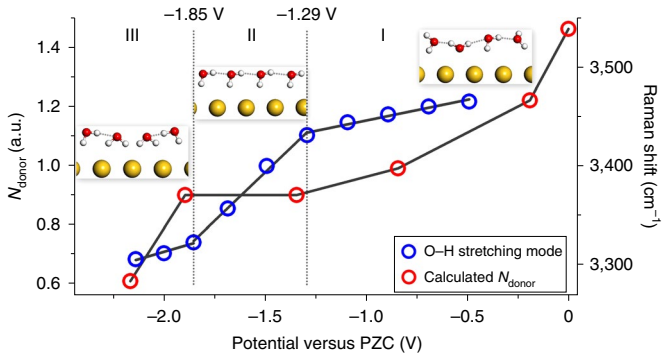

Fig. 4 | Potential-dependent evolution of the hydrogen-bond network of interfacial water. Calculated number of hydrogen-bond donors (N_{donor}) of interfacial water molecules (red circles) as a function of potential, in comparison to the experimental Raman frequency $\nu_{O\text{-}H}$ (blue circle). A hydrogen bond is defined when the O–O distance is shorter than 3.5 Å and the O–O–H angle is less than 35°. Insets, structure models of interfacial water in the corresponding potential regions.

water to 'one-H-down', and lead to an increase in the Raman intensity, which agrees well with the observed intensity change of the trihedrally coordinated water at −0.29 and −1.3 V in Fig. 2c. As for the tetrahedrally coordinated water, one would expect a similar change in its orientation and thus Raman intensity in response to the potential (peak 1 in Fig. 2c).

Interestingly, we find that in region II (−1.3 to ~−1.9 V) the interfacial water structure, including density distribution, orientation and N_{donor} (Figs. 3 and 4), hardly changes; that is, all water maintains the 'one-H-down' configuration. Shifting to even more negative potentials, we observe that a fraction of 'one-H-down' water starts to reorient to a 'two-H-down' configuration. The latter features φ peaked at ~160° and θ peaked at only ~145°. The φ and θ distributions at −2.16 V in Fig. 3b suggest the coexistence of 'one-H-down' and 'two-H-down' configurations. Concurrently, the N_{donor} further decreases to ~0.6 at −2.16 V, which indicates that 'one-H-down' and 'two-H-down' configurations are of nearly equal abundance at this potential, as 'one-H-down' water donates one hydrogen bond while 'two-H-down' water donates none (inset of Fig. 4).

Clearly, there is a good correlation between the potential dependence of N_{donor} and $\nu_{O\text{-}H}$ of the interfacial water (Fig. 4), which can be rationalized as follows. It is known that hydrogen bond donation can considerably change the $\nu_{O\text{-}H}$ of water, where decreasing N_{donor} can induce a blueshift of $\nu_{O\text{-}H}$ (ref. [27]). On the other hand, the Stark effect leads to a redshift of the $\nu_{O\text{-}H}$ of interfacial water at negatively charged metal surfaces, giving the general decreasing trend of $\nu_{O\text{-}H}$ when the potential shifts to negative (Fig. 2e). The Stark effect is somewhat compensated by a decrease in N_{donor} in regions I and III, that is, smaller slopes than in region II where N_{donor} remains constant.

To conclude, by combining in situ Raman spectroscopy measurements and AIMD simulations we have revealed the evolution of three characteristic water configurations ('parallel', 'one-H-down' and 'two-H-down' water) at a well-defined atomically flat Au single-crystal surface during a potential sweep. The experimentally observed potential dependence of the apparent Stark tuning rate of the O–H vibrational frequency of the interfacial water can be reproduced by AIMD simulations of electrified interfaces, which further demonstrate how such dependence is related to the change of orientation and hydrogen bonding of interfacial water in EDLs. Our study lays the foundation for future exploration of water-related fields, such as photochemistry, surface science, energy and materials science.

Online content

Any methods, additional references, Nature Research reporting summaries, source data, extended data, supplementary information, acknowledgements, peer review information; details of author contributions and competing interests; and statements of data and code availability are available at https://doi.org/10.1038/s41563-019-0356-x.

Received: 26 October 2018; Accepted: 25 March 2019;
Published online: 29 April 2019

References

1. Schmickler, W. & Santos, E. *Interfacial Electrochemistry* (Springer, 2010).
2. Nørskov, J. K. et al. Origin of the overpotential for oxygen reduction at a fuel-cell cathode. *J. Phys. Chem. B* **108**, 17886–17892 (2004).
3. Casalongue, H. S. et al. Direct observation of the oxygenated species during oxygen reduction on a platinum fuel cell cathode. *Nat. Commun.* **4**, 2817 (2013).
4. Ledezma-Yanez, I. et al. Interfacial water reorganization as a pH-dependent descriptor of the hydrogen evolution rate on platinum electrodes. *Nat. Energy* **2**, 17031 (2017).
5. Toney, M. F. et al. Voltage-dependent ordering of water molecules at an electrode–electrolyte interface. *Nature* **368**, 444–446 (1994).
6. Scatena, L. F., Brown, M. G. & Richmond, G. L. Water at hydrophobic surfaces: weak hydrogen bonding and strong orientation effects. *Science* **292**, 908–912 (2001).
7. Carrasco, J., Hodgson, A. & Michaelides, A. A molecular perspective of water at metal interfaces. *Nat. Mater.* **11**, 667–674 (2012).
8. Velasco-Velez, J.-J. et al. The structure of interfacial water on gold electrodes studied by X-ray absorption spectroscopy. *Science* **346**, 831–834 (2014).
9. Guo, J. et al. Real-space imaging of interfacial water with submolecular resolution. *Nat. Mater.* **13**, 184–189 (2014).
10. Wernet, P. et al. The structure of the first coordination shell in liquid water. *Science* **304**, 995–999 (2004).
11. Myneni, S. et al. Spectroscopic probing of local hydrogen-bonding structures in liquid water. *J. Phys. Condens. Matter* **14**, L213 (2002).
12. Ataka, K.-i, Yotsuyanagi, T. & Osawa, M. Potential-dependent reorientation of water molecules at an electrode/electrolyte interface studied by surface-enhanced infrared absorption spectroscopy. *J. Phys. Chem.* **100**, 10664–10672 (1996).
13. Liu, W.-T. & Shen, Y. R. In situ sum-frequency vibrational spectroscopy of electrochemical interfaces with surface plasmon resonance. *Proc. Natl Acad. Sci. USA* **111**, 1293–1297 (2014).
14. Schultz, Z. D., Shaw, S. K. & Gewirth, A. A. Potential dependent organization of water at the electrified metal–liquid interface. *J. Am. Chem. Soc.* **127**, 15916–15922 (2005).
15. Li, J. F. et al. Shell-isolated nanoparticle-enhanced Raman spectroscopy. *Nature* **464**, 392–395 (2010).
16. Chen, Y. X., Zou, S. Z., Huang, K. Q. & Tian, Z. Q. SERS studies of electrode/electrolyte interfacial water part II—librations of water correlated to hydrogen evolution reaction. *J. Raman Spectrosc.* **29**, 749–756 (1998).
17. Tong, Y., Lapointe, F., Thämer, M., Wolf, M. & Campen, R. K. Hydrophobic water probed experimentally at the gold electrode/aqueous interface. *Angew. Chem. Int. Ed.* **56**, 4211–4214 (2017).
18. Du, Q., Freysz, E. & Shen, Y. R. Vibrational spectra of water molecules at quartz/water interfaces. *Phys. Rev. Lett.* **72**, 238–241 (1994).
19. Nihonyanagi, S. et al. Potential-dependent structure of the interfacial water on the gold electrode. *Surf. Sci.* **573**, 11–16 (2004).
20. Tian, Z.-Q., Ren, B., Chen, Y.-X., Zou, S.-Z. & Mao, B.-W. Probing electrode/electrolyte interfacial structure in the potential region of hydrogen evolution by Raman spectroscopy. *J. Chem. Soc. Faraday Trans.* **92**, 3829–3838 (1996).
21. Le, J., Iannuzzi, M., Cuesta, A. & Cheng, J. Determining potentials of zero charge of metal electrodes versus the standard hydrogen electrode from density-functional-theory-based molecular dynamics. *Phys. Rev. Lett.* **119**, 016801 (2017).
22. Cheng, J., Liu, X., VandeVondele, J., Sulpizi, M. & Sprik, M. Redox potentials and acidity constants from density functional theory based molecular dynamics. *Acc. Chem. Res.* **47**, 3522–3529 (2014).
23. Kolb, D. M. & Schneider, J. Surface reconstruction in electrochemistry: Au(100-(5×20), Au(111)-(1×23) and Au(110)-(1×2). *Electrochim. Acta* **31**, 929–936 (1986).
24. Noguchi, H., Okada, T. & Uosaki, K. Molecular structure at electrode/electrolyte solution interfaces related to electrocatalysis. *Faraday Discuss.* **140**, 125–137 (2009).
25. Wasileski, S. A., Koper, M. T. M. & Weaver, M. J. Field-dependent electrode–chemisorbate bonding: sensitivity of vibrational Stark effect and binding

energetics to nature of surface coordination. *J. Am. Chem. Soc.* **124**, 2796–2805 (2002).
26. Moskovits, M. Surface-enhanced spectroscopy. *Rev. Mod. Phys* **57**, 783–826 (1985).
27. Scherer, J. R. in *Advances in Infrared and Raman Spectroscopy* Vol. 5 (eds Clark, R. J. H. & Hester, R. E.) Ch. 3 (Wiley, 1978).

Acknowledgements

The authors thank J.W. Yan and S. Liu for helpful discussions. Funding was provdied by the National Natural Science Foundation of China (grants nos. 21373166, 21775127, 21861132015, 21522508, 21521004, 21427813, 21321062, 21621091 and 21533006).

Author contributions

J.F.L., J.C., C.Y.L. and J.B.L. conceived and designed the project, analysed the results and wrote the manuscript. C.Y.L., Y.H.W., Z.Q.T. and J.F.L. carried out the experiments and analysed the data. J.B.L. and J.C. performed the AIMD calculations. Z.L.Y. and S.C. contributed to FDTD simulations.

Competing interests

The authors declare no competing interests.

Additional information

Supplementary information is available for this paper at https://doi.org/10.1038/s41563-019-0356-x.

Reprints and permissions information is available at www.nature.com/reprints.

Correspondence and requests for materials should be addressed to J.-F.L. or J.C.

Publisher's note: Springer Nature remains neutral with regard to jurisdictional claims in published maps and institutional affiliations.

Methods

Experimental methods. Au SHINs were prepared according to ref. [15] (see Supplementary Information for details). The Au single-crystal electrodes were Clavilier-type half-bead single-crystal electrodes. A scanning electron microscopy image of the Au(111) electrode surface-modified with SHINs is provided in Supplementary Fig. 1a.

Electrochemical Raman experiments were performed on a LabRam HR800 confocal Raman microscope (HORIBA JobinYvon) with a ×50 objective. Excitation at 633 nm was provided by a He-Ne laser (power of ~10 mW). A home-made spectroelectrochemical cell was used with a Pt wire counterelectrode and Ag/AgCl reference. Before experiments, the electrolyte was de-aerated with Ar gas. The ohmic drop in the thin-layer cell at very negative potentials was compensated for each spectrum provided in the main text and Supplementary Information. Finally, all potentials were referenced with respect to the corresponding PZC (0.29 and 0.13 V versus Ag/AgCl for Au(111) and Au(100) electrodes, respectively[23]).

Computational models and methodology. The Au(111) surface was modelled by a $p(4\times4)$ slab with six atomic layers, and a 21 Å water layer was added between the Au slabs to form two symmetric Au(111)/water interfaces in a periodic supercell. The EDLs were constructed by inserting Na^+ ions ~3 Å away from the Au surface (Stern layer). As our models were kept charge neutral, the surface charge density could be controlled by varying the number of Na^+ ions inserted. AIMD simulations were performed using the freely available CP2K/Quickstep[28] package. The Perdew–Burke–Ernzerhof density functional[29] with the Grimme D3 dispersion correction was used[30]. All AIMD models were first pre-equilibrated and then run for production periods of over 10 ps.

Data availability

The data that support the findings of this study are available from the corresponding author on reasonable request.

References

28. VandeVondele, J. et al. Quickstep: fast and accurate density functional calculations using a mixed gaussian and plane waves approach. *Comput. Phys. Commun.* **167**, 103–128 (2005).
29. Perdew, J. P., Burke, K. & Ernzerhof, M. Generalized gradient approximation made simple. *Phys. Rev. Lett.* **77**, 3865–3868 (1996).
30. Grimme, S., Antony, J., Ehrlich, S. & Krieg, H. A consistent and accurate ab initio parametrization of density functional dispersion correction (DFT-D) for the 94 elements H-Pu. *J. Chem. Phys.* **132**, 154104 (2010).